Rupture Directivities of the 2003 Big Bear Sequence

Ying Tan, Francisco Ortega and Don Helmberger

Seismological Laboratory, California Institute of Technology, Pasadena, California 91125

1 Abstract

We have developed a forward modeling technique to retrieve rupture characteristics of small earthquakes ($3 < M < 5$), including rupture propagation direction, fault dimension, and rupture speed. The technique is based on an empirical Green's function (EGF) approach, where we use data from co-located smaller events as Green's functions to study the bigger events. Compared to deconvolution, this forward modeling approach allows full use of both the shape and amplitude information produced by rupture propagation. Assuming simple 1D Haskell source model (*Haskell*, 1964), we parameterize the source time function of a studied event as the convolution of two boxcars, featuring the rise time τ_1 and the rupture time τ_2, and we solve for τ_1 and τ_2 in a grid search manner by minimizing the waveform misfit between the three-component data and the "synthetics" from the EGFs. By fitting the observed azimuthal pattern of τ_2 with the predictions from the model $\tau_2 = fl/V_{rup} - fl/V_c * \cos(\varphi - \phi)$, the fault length ($fl$) and rupture velocity ($V_{rup}$) can be estimated. We have applied the approach to the 11 strike slip events with magnitude greater than 3.4 of the 2003 Big Bear sequence. We generally chose smaller events with similar focal mechanisms for EGFs, however, we show that the smaller events with different focal mechanisms can work equally well if the radiation pattern effect can be appropriately corrected. The studied events show rupture propagation in all directions with wide-ranged rupture speeds (1.5–3.5 km/sec), implying the complexities of conjugate faulting.

2 Introduction

The direct consequence of rupture propagation on a fault plane is the azimuthal dependence of the observed source time function (STF). In brief, if a seismic station is located along the rupture propagation direction, the STF is narrower and has a higher amplitude. In contrast, for a station located such that the rupture is propagating away from it, the STF will be spread out and have a smaller amplitude. Many previous investigations using deconvolution have been focused on the duration variations of the STFs, whereas the amplitude information was somewhat ignored. An example of the amplitude signal due to rupture directivity is diplayed in Figure 1. To fully utilize both the duration and amplitude signals due to rupture propagation, we propose a forward modeling approach to retrieve STFs. Moreover, provided corrections for the difference in the events' radiation patterns (Figure 2), empirical Green's functions (EGFs) can be obtained from events with different focal mechanisms.

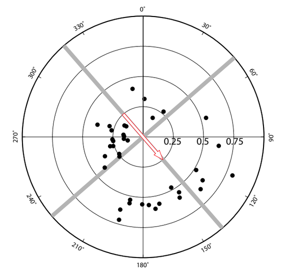

Figure 1: The vertical P wave amplitude ratios, Amp_{7632}/Amp_{74922} between the event 13937632 ($M \sim 2.5$) and 13937492 ($M \sim 3.5$). The two events have similar strike slip focal mechanisms (Fig. 3). The gray lines indicate the strikes of their fault planes. Note the amplitude ratios for the southeastern stations are consistently larger than those for the northwestern stations, due to the rupture directivity effect of the bigger event.

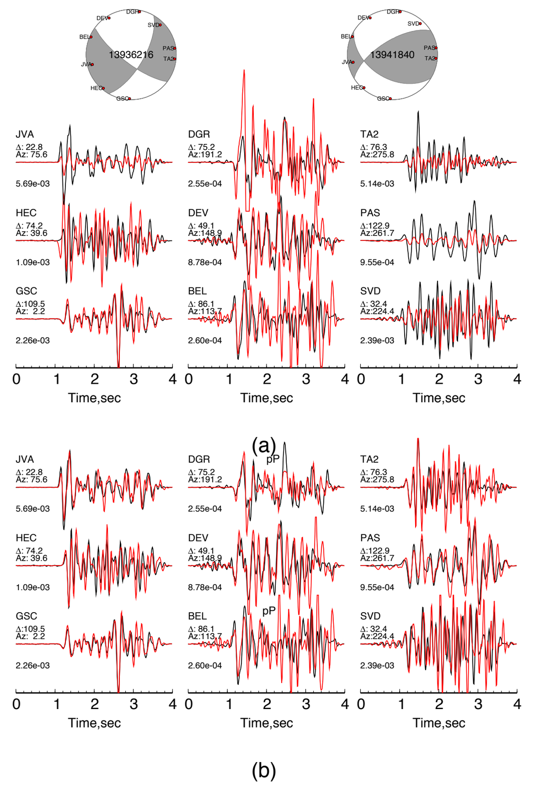

Figure 2: The focal mechanisms of the strike-slip event (13936216) and the thrust event (13941840) together with the selected stations sampling the whole azimuthal range. The records from these stations of the two events (13936216: black; 13941840: red) will be compared in (a) and (b). A band-pass filter (0.5-10 Hz) has been applied and the amplitudes of the traces have been normalized by the factors below them. Particularly in (b), the records of the thrust event (13941840) have been multiplied by simple amplitude and polarity corrections derived from synthetics, to account for the two events' differences in radiation patterns.

3 Methodology

Let $d(t)$ and $g(t)$ be the records from a large event ($Mw > 3.5$) and the associated EGF event at the same station, which can be related by the relative source time function, $RSTF(t)$ of the large event as:

$$d(t) = g(t) * RSTF(t). \tag{1}$$

Assuming a simple trapezoidal shape of $RSTF(t)$ according to the 1D Haskell model, where $RSTF(t)$ can be parameterized as the convolution of two boxcars, featuring the rise time τ_1 and the rupture time τ_2, we can solve for $RSTF(t)$ in a grid search manner by minimizing the misfit defined as:

$$e = \|d(t) - \Delta M_0 g(t) * RSTF(t)\|, \tag{2}$$

$$\text{where } RSTF(t) = \tau_1(t) * \tau_2(t). \tag{3}$$

Here the parallels denote the L_2 norm. ΔM_0 is an amplitude scaling factor to account for the two events' difference in size and radiation pattern.

We first use the event 13937492 to illustrate the whole process (Figure 4 and 3), and more results of other studied events will be following.

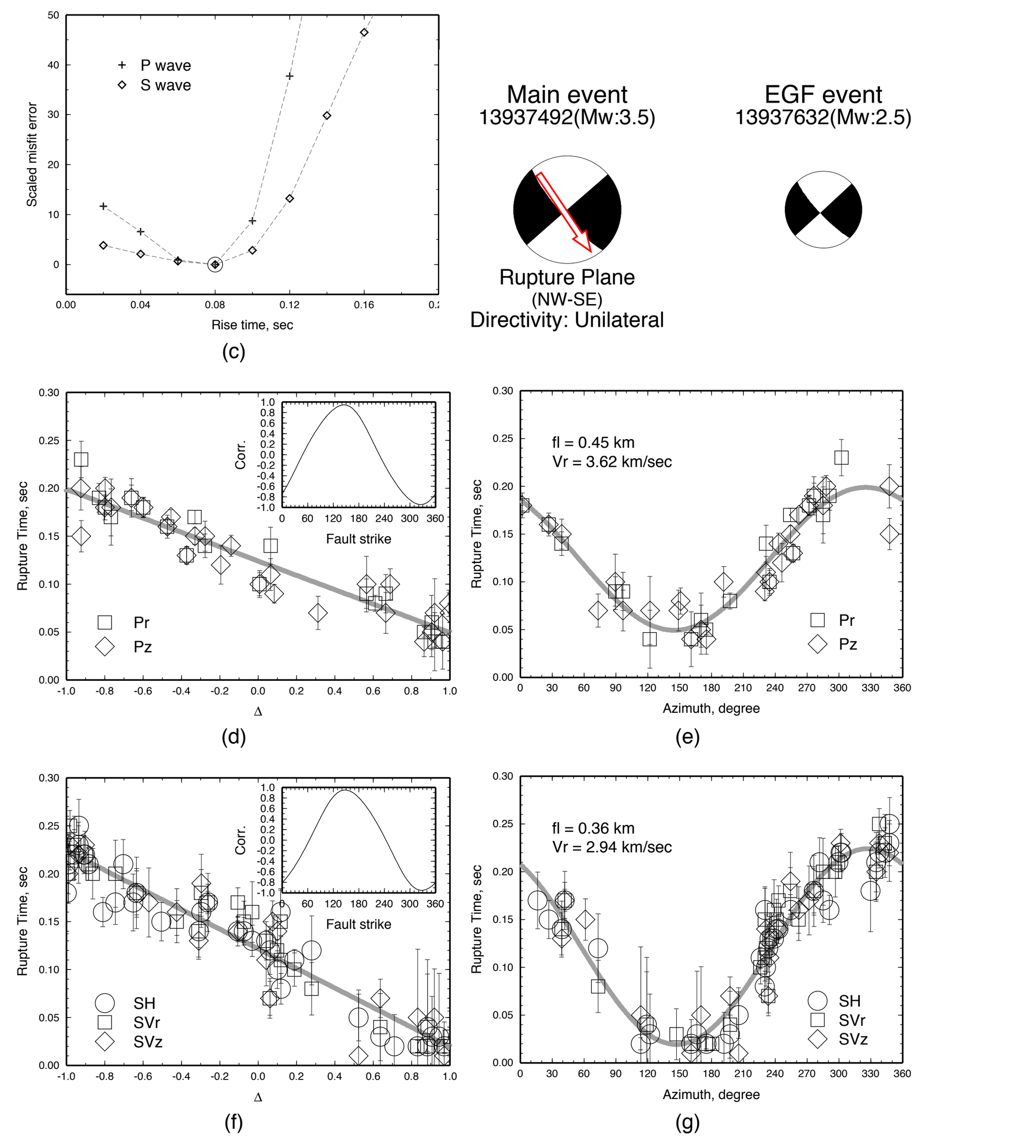

Figure 3: (a) The summation of misfit errors as defined in Eq. 3 from all the stations scaled by their minima *vs.* rise time τ_1. The best estimate of τ_1 occurs where the total misfit errors approache the minima, in this case, 0.08 sec. (b) The τ_2 estimates from P waves *vs.* Δ ($\Delta = \cos(\varphi - \phi_0)$) from the preferred rupture propagation direction ϕ_0. ϕ_0 is chosen where the linear cross-correlation coefficient between τ_2 and Δ reaches the maximum (see the inset). The plotted data points are associated with waveform cross-correlation values greater than 85 between the records from the main event (13937492) and the EGF event (13937632) convolved with the RSTFs. The uncertainties of the τ_2s are estimated by a 10% decrease in variance reduction. The grey line displays the linear least-squares fit between τ_2 and Δ, from which fault length (fl) and rupture speed (V_{rup}) can be estimated (c) τ_2 *vs.* azimuth. (d) and (e) display the results from S waves.

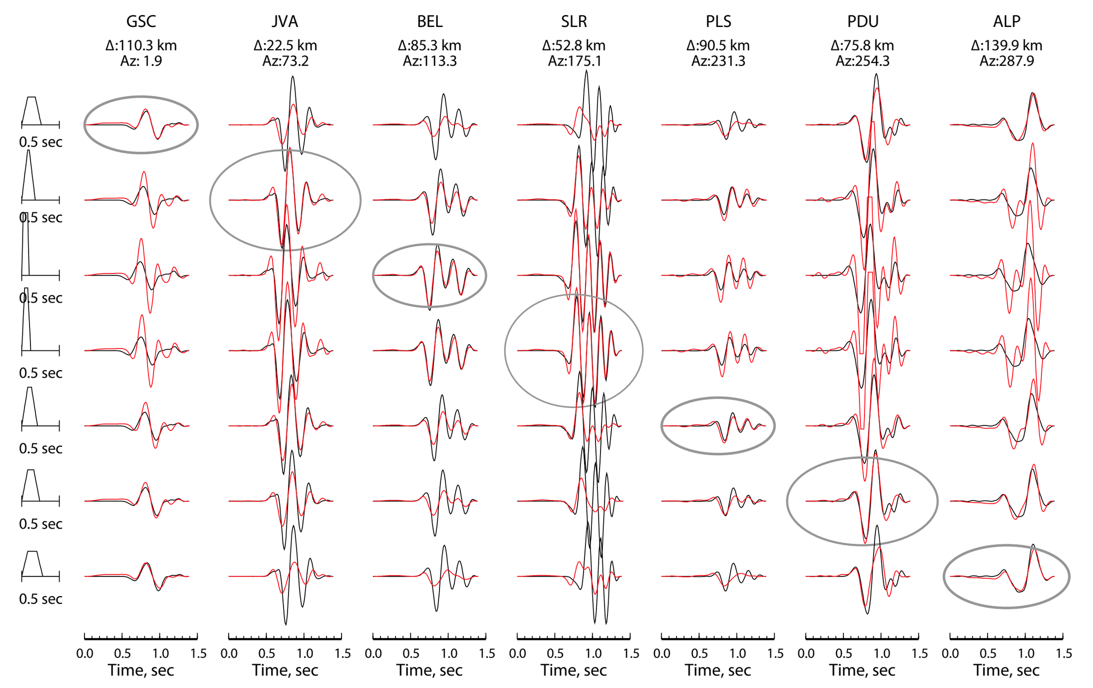

Figure 4: The selected waveform fits (vertical P waves) between the records from event 13937492 (black) and the "synthetics" (red) constructed with EGFs from event 13937632. The relative source time functions (RSTFs) are given to the left. Plotted are the absolute amplitudes, except that a scaling factor of 1/4, 1/2 and 2 has been applied to the stations JVA, PDU and PLS respectively for the display purpose. The obtained best RSTFs for the stations are circled. Note the apparent azimuthal pattern of the RSTFs.

4 Results

Figures 5–8 display more results for the events that rupture unilaterally. Please see the caption of Figure 3 for explannations. Particularly, we display in Fig. 9 the questionable result for the event 13939856, where the linear correlation between rupture time and Δ drops below 0.7, and the azimuthal pattern becomes obscure. Such lack of rupture directivity might suggest the ruptured area has a circular geometry or a large vertical dimension.

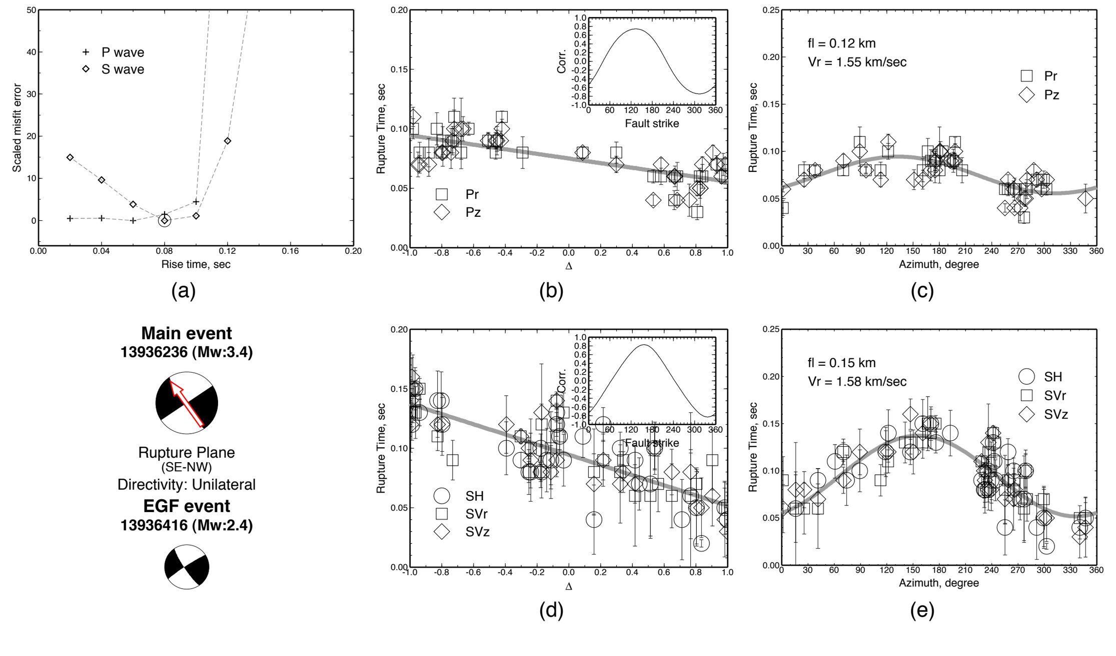

Figure 5: Event 13936236.

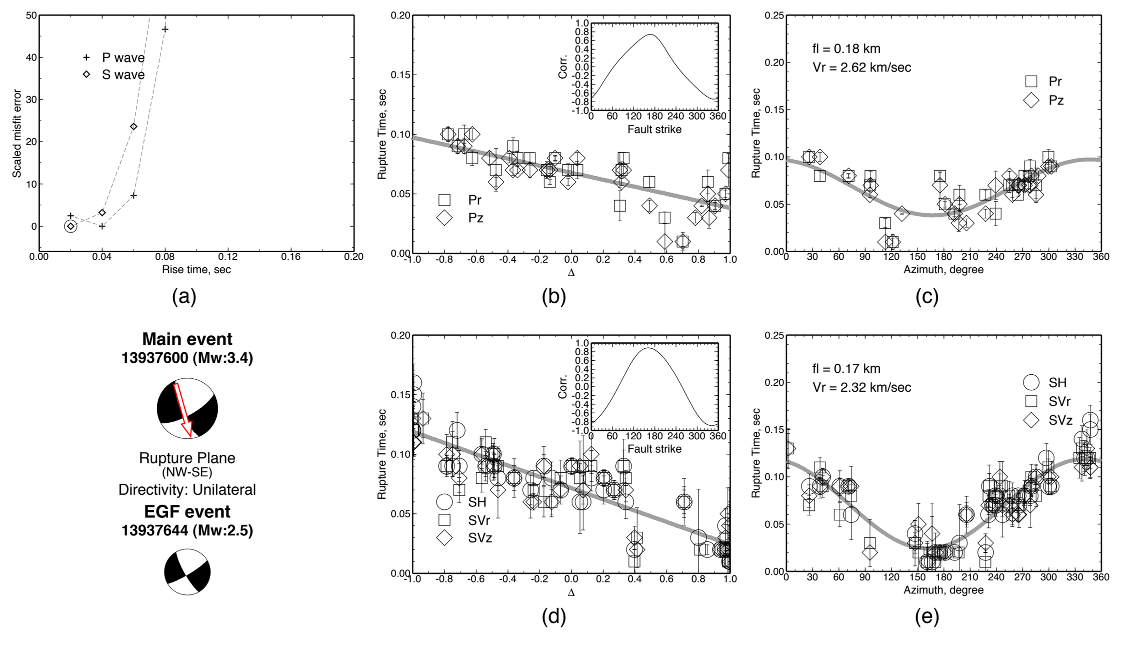

Figure 6: Event 13937600.

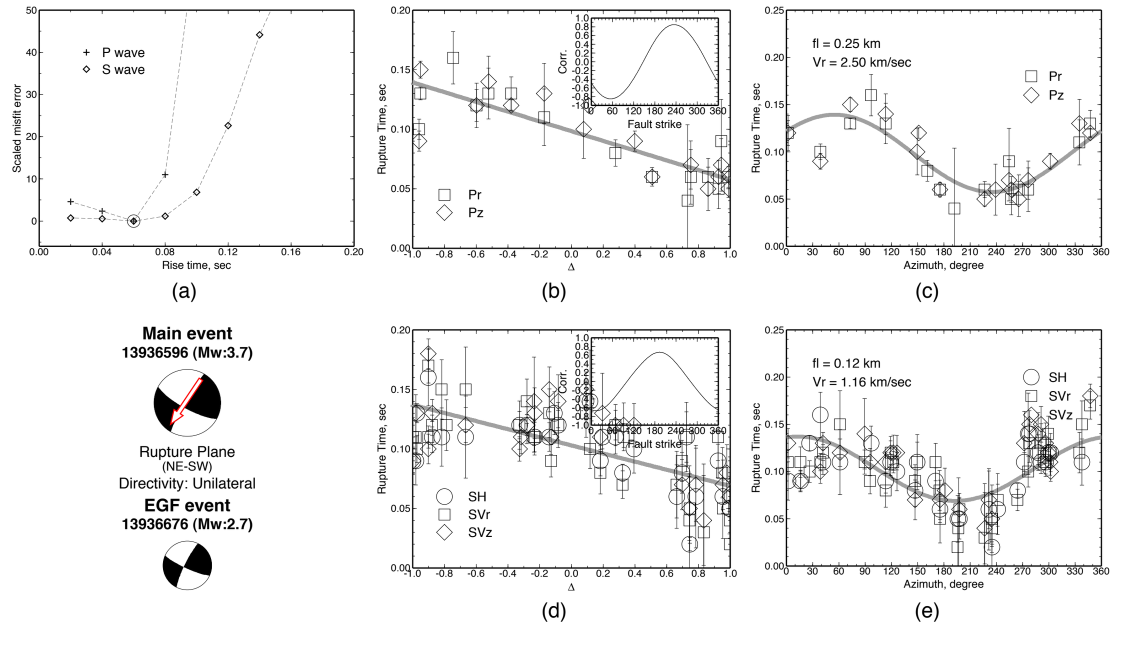

Figure 7: Event 13936596.

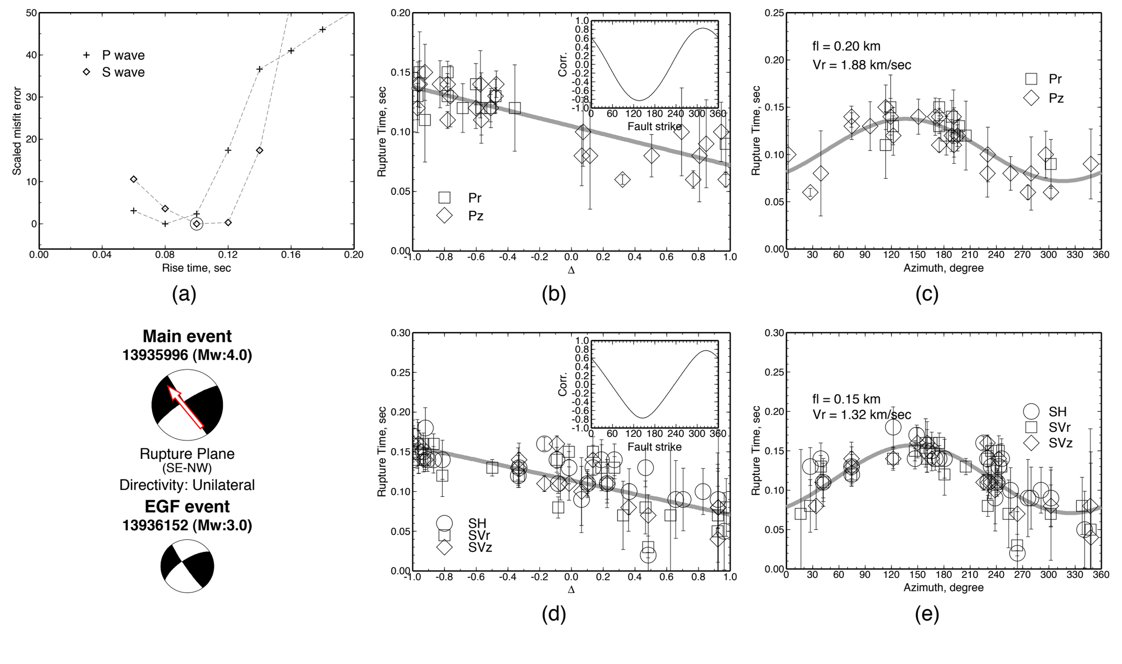

Figure 8: Event 13935996.

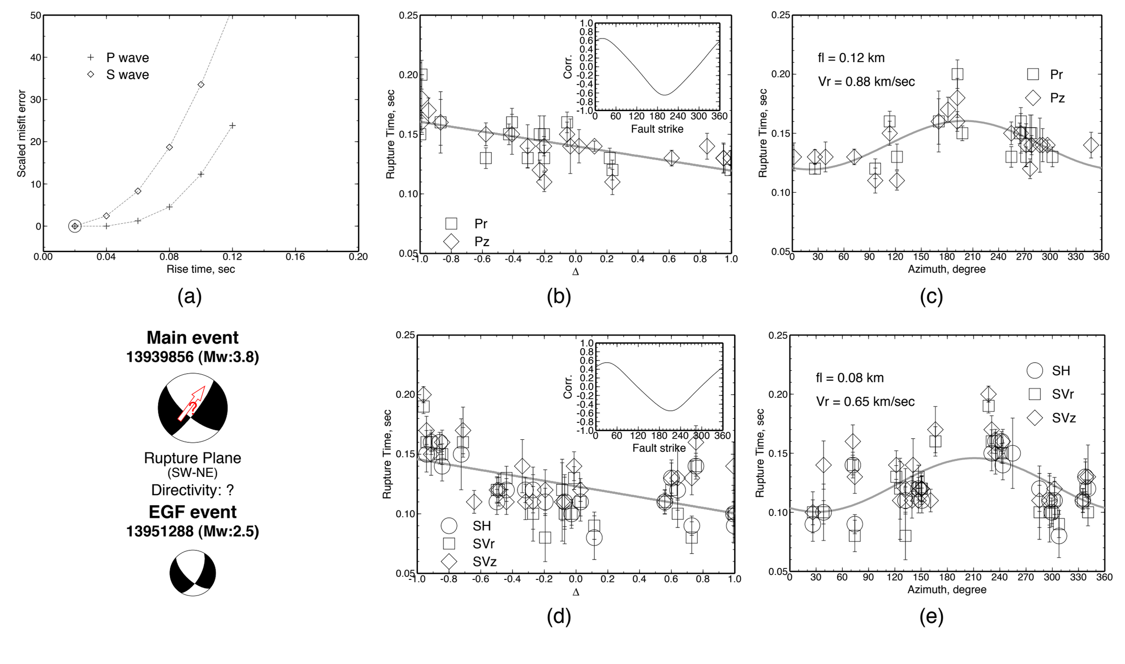

Figure 9: Event 13939856.

5 Discussion and Conclusions

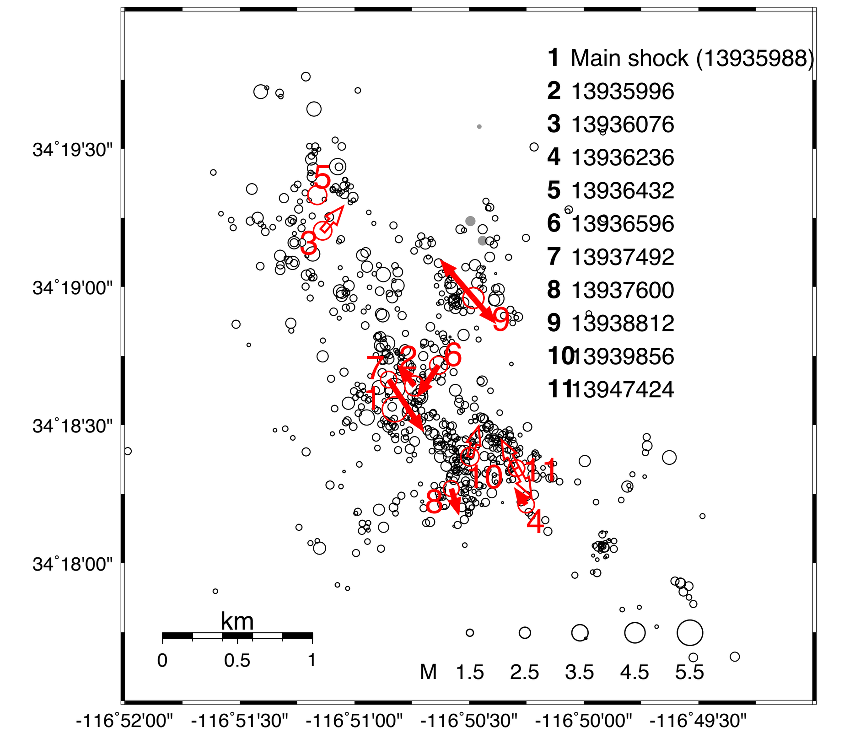

Figure 10: The inferred rupture directivities from our studied eventstogether with the relocated seismicity from Chi and Hauksson, *2006*. The arrows point to the rupture directions while their lengths (for the solid ones) indicate the fault lengths. Note that the ruptured planes correlate well with the seismicity lineations, suggesting cross-over faults at depth. The complex pattern of propagation direction warrants investigations with simulation of rupture dynamics.

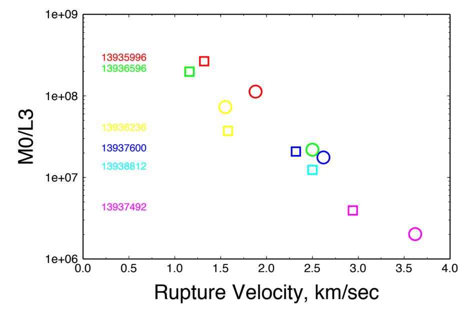

Figure 11: $M0/L^3$ vs. rupture speed from the studied events. The squares are the measurments from S waves, and the circles are from P waves. The good linear correlation between $M0/L^3$ and V_r suggests that low stress drop events tend to propagate at high rupture speed, whereas high stress drop events tend to propagate at low rupture speed.